ACS APPLIED BIO MATERIALS Cite This: ACS Appl. Bio Mater. XXXX, XXX, XXX−XXX

Article

www.acsabm.org

# Computer-Aided Design of Nanoceria Structures as Enzyme Mimetic Agents: The Role of Bodily Electrolytes on Maximizing Their Activity

Marco Molinari,*[,†,‡] Adam R. Symington,[‡] Dean C. Sayle,[§] Tamil S. Sakthivel,[∥] Sudipta Seal,[∥,⊥] and Stephen C. Parker[‡]

[†]Department of Chemistry, University of Huddersfield, Queensgate, Huddersfield HD1 3DH, United Kingdom

[‡]Department of Chemistry, University of Bath, Claverton Down, Bath BA2 7AY, United Kingdom

[§]School of Physical Sciences, University of Kent, Canterbury, Kent CT2 7NH, United Kingdom

[∥]Department of Materials Science and Engineering, Advanced Materials Processing and Analysis Center, Nanoscience and Tehcnology Center, University of Central Florida, Orlando, Florida 32816, United States

[⊥]College of Medicine, University of Central Florida, Orlando, Florida 32827, United States

Supporting Information

**ABSTRACT:** Nanoceria, typically used for "clean-air" catalytic converter technologies because of its ability to capture, store, and release oxygen, is the same material that has the potential to be used in nanomedicine. Specifically, nanoceria can be used to control oxygen content in cellular environments; as a "nanozyme", nanoceria mimics enzymes by acting as an antioxidant agent. The computational design procedures for predicting active materials for catalytic converters can therefore be used to design active ceria nanozymes. Crucially, the ceria nanomedicine is not a molecule; rather, it is a crystal and exploits its unique crystal properties. Here, we use ab initio and classical computer modeling, together with the experiment, to design structures for nanoceria that maximize its nanozymetic activity. We predict that the optimum nanoparticle shape is either a (truncated) polyhedral or a nanocube to expose (active) $CeO_2${100} surfaces. It should also contain oxygen vacancies and surface hydroxyl species. We also show that the surface structures strongly affect the biological activity of nanoceria. Analogous to catalyst poisoning, phosphorus "poisoning", the interaction of nanoceria with phosphate, a common bodily electrolyte, emanates from phosphate ions binding strongly to $CeO_2${100} surfaces, inhibiting oxygen capture and release and hence its ability to act as a nanozyme. Conversely, the phosphate interaction with {111} surfaces is weak, and therefore, these surfaces protect the nanozyme against poisoning. The atom-level understanding presented here also illuminates catalytic processes and poisoning in "clean-air" or fuel-cell technologies because the mechanism underpinning and exploited in each technology, oxygen capture, storage, and release, is identical.

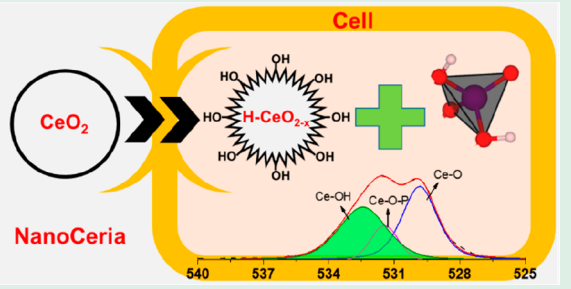


**KEYWORDS:** *cerium oxide nanoparticles, antioxidant, oxidative stress, phosphate, density functional theory, molecular dynamics, enzyme mimetic activity, prescription for therapeutic activity*



## INTRODUCTION

Nanotherapeutics employs technologies at the nanoscale and is one of the most promising routes to control oxidative stress, by inducing apoptosis of damaged cells.[1] Oxidative stress is a major factor of aging and life span[2] and is caused by the accumulation of highly reactive oxygen species (ROS) due to an insufficient buffering by antioxidant defenses.[3] ROS oxidize cell constituents such as lipids, proteins, and DNA, and compromise cell structures and functions. As such, oxidative stress has been related to chronic inflammations, cancer, and neurodegenerative and immune-deficient disorders.[4,5]

Nanoceria is a versatile, commercially valuable catalytic material with properties profoundly different from the parent bulk material. Nanoceria's activity can be tuned via synthetic protocol, particle size, nature and level of dopant, particle shape, and surface chemistry. Ceria has commercial utility in the areas of chemical mechanical polishing and planarization, catalytic converters and diesel oxidation catalysts, and intermediate temperature solid oxide fuel cells and sensors.[6] Its potential future uses include chemical looping combustion, photolytic and thermolytic water splitting for hydrogen production, and as a therapeutic agent for the treatment of certain human diseases.

Among nanotechnologies, nanozymes, metal oxide nanomaterials that display enzyme mimetic activity, have drawn great interest.[1,7−9] Nanoceria fits within this class of materials because of its remarkable redox activity arising from the easy conversion between oxidized $CeO_2$ and oxygen-deficient

Received: November 14, 2018
Accepted: January 23, 2019
Published: January 23, 2019




DOI: 10.1021/acsabm.8b00709
ACS Appl. Bio Mater. XXXX, XXX, XXX−XXX

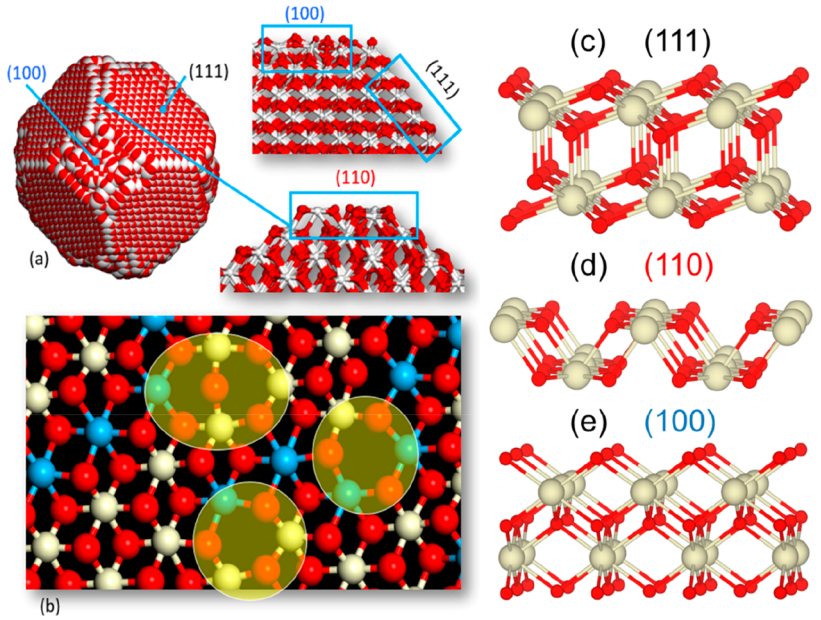


**Figure 1.** (a) Structure of a nanoparticle of ceria showing {111}, {110}, and {100} surfaces. (b) View of one of the nanoparticle's {111} surfaces after nanoceria has been reduced reveals oxygen vacancies residing on the surface as indicated by the yellow ovals. The structures of "perfect" (c) {111}, (d) {110}, and (e) {100} surfaces of nanoceria simulated using DFT are consistent with the structures of the surfaces exposed by the nanoparticle (a). $Ce^{4+}$ is white, $Ce^{3+}$ is blue, and oxygen is red.

$CeO_{2-x}$. This property enables nanoceria to act catalytically to capture, store, and release oxygen. Nanoceria has long been employed by the catalysis and energy industries,[6] but only recently was probed in biomedicine,[10−20] to protect against radiation-induced cellular damage,[21] anti-inflammatory[22] and antioxidant[13,23,24] agents, self-regulated bioassays,[25] growth promoter of stem cells,[26] protection agent in cardiovascular disease,[27,28] detection agent of cancer biomarkers,[2930] and therapeutic agent for retinal degeneration[31,32] and neuroprotection[33−35] including Alzheimer's disease.[36]

Nanoceria has many and competing enzyme mimetic activities, but the most important are those related to the suppression of ROS. At the nanoscale, surface defects, including oxygen vacancies and $Ce^{3+}$ ions, are responsible for the ROS scavenging activity of nanoceria, enabling it to mimic the activity of superoxide dismutase[14,37−39] and catalase.[13,39−43] Nanoceria exploitation in nanotherapeutics rests with its ability to capture, store, and release oxygen as much as in any other catalytic applications,[6] thus requiring control over those many factors influencing its activity, including particle size and morphology,[40] $Ce^{3+}/Ce^{4+}$ ratio, electrolyte species,[41] and pH.[16,20,36] Unlike clinical activity, which is focused on the physiological response of cells in the presence of nanoceria, here we focus on the design of the material to control mimetic activity.

The interaction of nanoceria with electrolyte species, which are abundant in cellular environments, has been largely overlooked, yet they may "poison" the nanoceria catalyst. A common inorganic anion is phosphate, which can interact with nanoceria surfaces and interfere with ROS scavenging.[41,42,44,45] However, the mechanisms underpinning phosphorus "poisoning" are unclear, as much as the poisoning and deactivation of catalysts by $SO_x$ are still big challenges in catalysis.[6] Here, we investigate phosphorus poisoning using both first-principles and classical modeling. We predict that, at the atomic level, the interaction is an intricate balance between the surface defect concentration (oxygen vacancies and $Ce^{3+}$) and hydroxyl groups adsorbed on the nanoceria surfaces. We discuss this in the context of the most suitable nanoceria morphologies for reducing the interference of phosphate with ROS scavenging activity. Such understanding will also provide insight into poisoning of ceria nanocatalysts exploited for other applications, such as clean-air and energy materials (fuel-cell) technologies.[6]

## METHODOLOGY

**Quantum Mechanics.** Density functional theory (DFT) calculations were performed using the Vienna Ab initio Simulation Package (VASP),[46,47] within which projector augmented wave pseudopotentials and a plane wave cutoff of 500 eV were used. Calculations were carried out using the generalized gradient approximation (GGA) exchange-correlation functional of Perdew, Burke and Ernzerhof revised for solids (PBEsol),[48] with the +U correction of Dudarev[49] to account for on-site Coulombic interactions. A U value of 5 eV is applied to Ce f states.[50]

The structures were geometrically optimized until the residual forces on each atom were less than 10 meV $Å^{-1}$. All calculations were spin polarized, and a ferromagnetic ordering was used throughout, which was shown to bare no difference in the energetic of $CeO_2$ systems. The details of model structures are provided in the Supporting Information.

**Classical Mechanics.** A model nanoparticle of $CeO_2$ comprising 18 849 atoms was generated using simulated amorphization and crystallization; details of this strategy can be found in ref 51. During crystallization, the structure of the nanoparticle evolves exposing {111}, {110}, and {100} surfaces in accord with the real nanomaterial. A total of 628 oxygen vacancies (together with 1256 $Ce^{3+}$ for charge balance) were then randomly introduced into the model nanoparticle, and MD simulation was run, at 2000 K, for 2.5 ns. This relatively high temperature MD simulation was performed to


DOI: 10.1021/acsabm.8b00709
ACS Appl. Bio Mater. XXXX, XXX, XXX−XXX

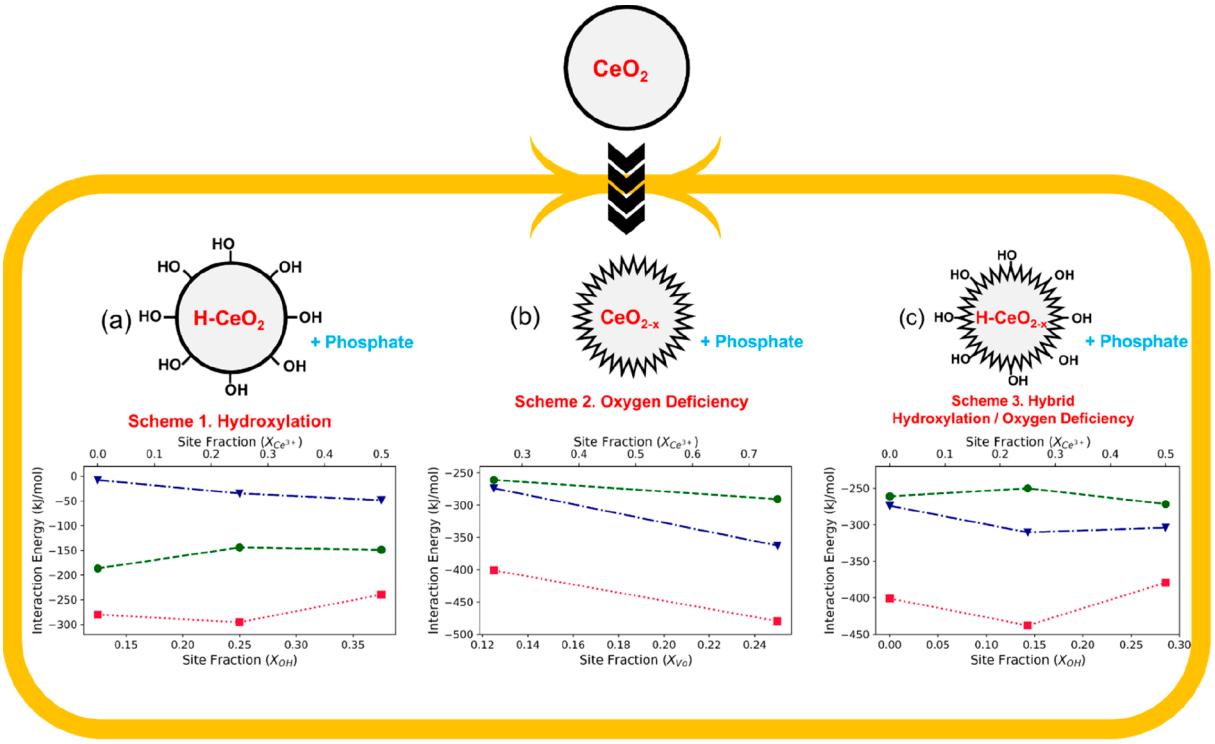


**Figure 2.** Interaction energy of phosphate with nanoceria for three compositions of nanoceria in a living cell. Interaction energy (kJ/mol) of phosphate at nanoceria surfaces {111} (blue triangles), {110} (green circles), and {100} (red squares), (a) Scheme 1, as a function of coverage of $OH^-$ and $Ce^{3+}$ on hydroxylated oxygen stoichiometric surfaces; (b) Scheme 2, as a function of coverage of Vo and $Ce^{3+}$ oxygen-deficient surfaces; (c) Scheme 3, as a function of coverage of $OH^-$ and $Ce^{3+}$ on hydroxylated oxygen-deficient surfaces.

enable the oxygen vacancies to locate to low energy equilibrium positions within the nanoparticle (including on the nanoparticle surface); the nanoparticle was then cooled. Inspection of the model revealed the presence of oxygen vacancies, which reside throughout the nanoparticle and also on the surface, Figure 1.

**Nanoparticle Preparation.** Bare nanoceria particles were synthesized according to the previously described procedure.[52,53] Typically, an appropriate amount of cerium(IV) ammonium nitrate was dissolved in DI water, and the reaction was carried out at 100 °C under reflux conditions with continuous stirring. An appropriate amount of ammonium hydroxide was added slowly to the equilibrated solution mixture, and the reaction was continued for 24 h to obtain $CeO_2$ nanoparticle dispersion.

**Phosphate Ion Treatment.** The phosphate ion buffer solution was prepared by mixing the 1:1 ratio of a 50 mM aqueous solution of $Na_2HPO_4$ and 50 mM aqueous solution of $NaH_2PO_4$. The molar ratio of phosphate ion buffer solution and nanoparticle was maintained as 4:1, and the incubation period was 24 h. The treated nanoparticles were separated by multiple centrifugation for XPS analysis.

**Characterization.** The particle size was measured using high-resolution transmission electron microscopy (HRTEM) (FEI Technai F30 TEM), at a potential of 300 kV. The selected areas electron diffraction (SAED) pattern was used to analyze the crystallinity of nanoparticles. The analysis of the electronic/vacancy state of nanoceria was completed with the use of an X-ray photoelectron spectrophotometer. The instrument used was a Physical Electronics 5400 ESCA using unmonochromatized Mg K$\alpha$ × (1253.6 eV) ray sources. The experiments were all conducted at ultrahigh vacuum (UHV) with a maximum internal pressure of $5 \times 10^{-8}$ Torr within the instrument. The spectra observed are comparative standards that we have used to analyze the change in the surface chemistry of cerium, oxygen, and phosphorus under their new chemical configuration. The spectra have all been referenced and shifted to the carbon peak position at 284.5 eV in order to compensate for charging due to irradiation.

## RESULTS

**Nanoceria Morphology.** The calculated nanoceria equilibrium morphology is a truncated octahedron expressing {111}, {100}, and {110} surfaces and was first found using simulated amorphization and recrystallization (Figure 1).[51] The surface structure (Figure 1a,c,d,e), surface reduction (Figure 1b),[54] and surface hydroxylation[50,55] all influence the catalytic performance of nanoceria and are therefore central to our first principle analysis and design of schemes (Figure 2) that we use to disentangle the role of phosphate on nanoceria surfaces. These schemes are constructed to represent possible experimental routes that nanoceria will undergo during cellular uptake and are based on the experimental evidence that phosphate adsorption increases surface $Ce^{3+}$ concentration. Figure 2 also includes the diagrams for the interaction energy of phosphate, which describes the strength of the interaction between the phosphate species and the different nanoceria {111}, {110}, and {100} surfaces. The interaction energy is presented for Scheme 1 (nanoceria hydroxylated oxygen stoichiometric surfaces) as a function of surface concentrations of hydroxyl groups and $Ce^{3+}$, for Scheme 2 (nanoceria oxygen-deficient surfaces) as a function of surface concentrations of oxygen vacancies and $Ce^{3+}$, and for Scheme 3 (nanoceria hydroxylated oxygen-deficient surfaces) as a function of surface


DOI: 10.1021/acsabm.8b00709
ACS Appl. Bio Mater. XXXX, XXX, XXX−XXX

concentrations of hydroxyl groups and $Ce^{3+}$. These schemes are explained in detail hereafter.

*Phosphate Adsorption on Hydroxylated Stoichiometric Ceria Surfaces.* Figure 2a represents Scheme 1, which considers the adsorption of phosphate on hydroxylated, oxygen stoichiometric surfaces of nanoceria. In this scenario the ratio of $Ce^{3+}/Ce^{4+}$ is governed only by the concentration of surface hydroxyl groups ($x_{OH}$), and as this increases, the concentration of $Ce^{3+}$ increases.

Figure 2a shows the strength of the interaction between phosphate and nanoceria when its surfaces are hydroxylated. The preferential affinity of phosphates follows the order {100} > {110} > {111} as the more negative energy terms indicate the strongest interaction. We observe that, across the majority of our ab initio calculations, phosphate adsorbs with a tridentate geometry (Figure 3a), enabling surface Ce atoms

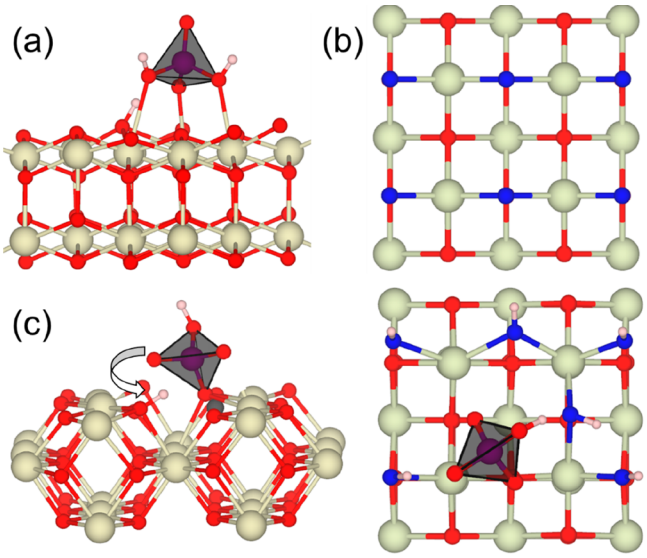


**Figure 3.** Examples of (a) phosphate adsorbed with a tridentate geometry on the {111} surface of nanoceria, (b) reconstruction of the outer oxygen layer on the {100} surface of nanoceria when phosphate is adsorbed, and (c) phosphate directly adsorbed on oxygen vacancies at the {110} surface of nanoceria associated with a barrierless dissociation (arrow) whereby a hydrogen adsorbs on a nearby surface oxygen. Ce is white, and oxygen is red. The outermost oxygen is blue in part b to show the surface reconstruction.

to recover the oxygen coordination, partially on the {110} and {100}, and fully on the {111} surface, which explains the order of energetic affinity. The strongest interaction occurs at the {100} surface, which undergoes a large surface reconstruction to accommodate the adsorbed phosphate (Figure 3b).

*Phosphate Adsorption on Surfaces with Oxygen Vacancies.* Figure 2b represents Scheme 2, which considers the adsorption of phosphates on oxygen deficient surfaces of nanoceria by introducing surface oxygen vacancies. The $Ce^{3+}/Ce^{4+}$ ratio is thus governed by the oxygen stoichiometry ($x_{Vo}$), i.e. as the concentration of oxygen vacancies increases so the concentration of $Ce^{3+}$ increases to maintain charge neutrality.

Figure 2b shows the interaction strength between phosphate and oxygen-deficient nanoceria. Here, the phosphate interacts strongly and directly with the surface oxygen vacancies by filling the vacant site (Figure 3c). This interaction becomes stronger as the surfaces become more defective (more $Ce^{3+}$ and oxygen vacancies). This mechanism has been proposed experimentally.[41,42,44,45,56,57] When oxygen vacancies are present on the surfaces of nanoceria, our ab initio calculations reveal a barrierless dissociative adsorption of phosphate whereby a hydrogen adsorbs on a nearby surface oxygen (Figure 3c).

Unlike on hydroxylated surfaces (Scheme 1), the strength of interaction between nanoceria and phosphate in Scheme 2 follows the order {100} > {111} > {110}. Although there is certainly a component due to the extent of recovery of surface Ce atoms coordination, this work shows that it also depends on the ease of removal of oxygen from the surface (i.e., heat of reduction), which follows the order {111} > {100} > {110}.[50] The adsorption of phosphate on oxygen-deficient surfaces is accompanied by an oxidative reaction of $Ce^{3+}$ to $Ce^{4+}$. As the {111} has a larger energy barrier to reduction (254.72 kJ/mol) compared to the {110} surface (177.53 kJ/mol), the {111} surface is easier to reoxidize and hence stabilize upon adsorption of phosphate. The anomaly is still the {100} surface, where the heat of reduction lies between the {111} and {110} surfaces (192.01 kJ/mol). This surface shows the strongest interaction because of the large surface reconstruction (Figure 4b), which overstabilizes the surface upon phosphate adsorption.

*Phosphate Adsorption on Hydroxylated Surfaces with Oxygen Vacancies.* Figure 2c represents Scheme 3, which is a hybrid scenario between Scheme 1 and Scheme 2, where the adsorption of phosphate on nanoceria oxygen deficient surfaces depends on hydroxylation. The ratio $Ce^{3+}/Ce^{4+}$ is governed by surface hydroxyl groups ($x_{OH}$) at a constant concentration of surface oxygen vacancies ($x_{Vo}$).

Similar to Scheme 2, in Scheme 3 (Figure 2c), the preferential affinity of phosphate follows the order {100} > {111} > {110}, with phosphate adsorbing directly onto oxygen vacancies displaying a barrierless dissociation (Figure 3b). We again see a large surface reconstruction of the {100} surface of nanoceria, which again makes this surface the most favorable for phosphate adsorption (Figure 3b).

**Experimental Surface Analysis of Nanoceria after Phosphate Ion Treatment.** Details of sample preparation and characterization and phosphate treatment are available in the Supporting Information. SAED patterns of the 8−10 nm synthesized nanoparticles (Figure 4a) reveal (111), (200), (220), and to a lesser extent (311) lattice planes, confirming a cubic fluorite $CeO_2$ structure.

To align with the modeling work, $Ce^{4+}$-rich nanoceria was treated with phosphate and targeted toward an early stage phosphate−ceria interaction; phosphate concentrations were controlled to prevent $CePO_4$ formation, and as in our calculations, the adsorption of phosphate promotes formation of $Ce^{3+}$. The spectra of cerium 3d, oxygen 1s, and phosphorus 2p of nanoceria particles before and after phosphate buffer treatment were obtained using high-resolution XPS (Figure 4b−d). Surface cerium ions in nanoceria are mostly $Ce^{4+}$ before (30% $Ce^{3+}$ and 70% $Ce^{4+}$) and after (43% $Ce^{3+}$ and 57% $Ce^{4+}$) phosphate treatment at neutral pH, although the $Ce^{3+}$ concentration increased 13% in the treated sample, resulting in a $Ce^{3+}$ concentration of 43% (Figure 4b). $Ce^{3+}$ concentrations can increase by as much as 21% with treated nanoceria, resulting in $Ce^{3+}$ concentrations of 80%.[45] Details of $Ce^{4+}$ and $Ce^{3+}$ concentrations are given in the Supporting Information.

Analysis of oxygen binding energies and peak structures before and after treatment shows predominant asymmetry for


DOI: 10.1021/acsabm.8b00709
ACS Appl. Bio Mater. XXXX, XXX, XXX−XXX

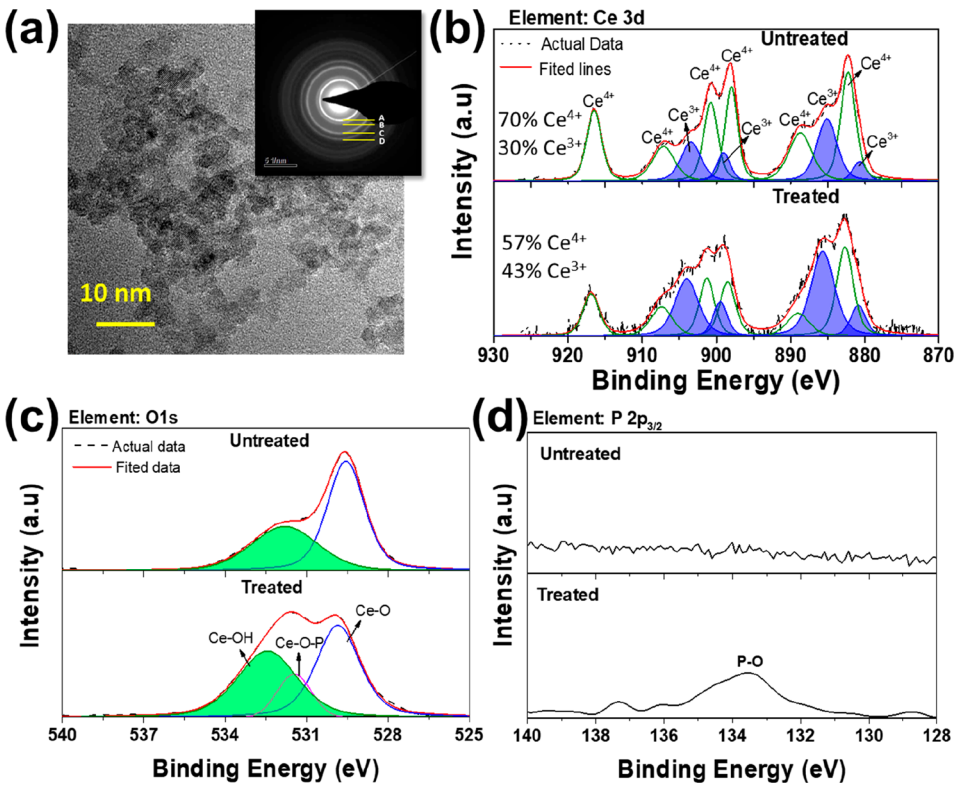


**Figure 4.** (a) TEM image of nanoceria with SAED patterns and the particle of 5−10 nm range. (A, B, C, and D are the 111, 200, 220, and 311 lattice planes.) (b−d) High-resolution XPS spectra of nanoceria before and after incubation with phosphate. (b) Ce 3d spectra: the concentration of $Ce^{3+}$ is increased after interaction with phosphate (~13%). (c) O 1s spectra: PO−Ce peak has formed in the treated sample. (d) P 2p spectra: intense emission in the 2p region was observed after treatment, which indicates the presence of phosphate on the surface of the nanoceria sample.

both treated and untreated nanoceria, which is attributed to surface CO (single or double bond formation) and hydroxide ($OH^-$) species. The absence of a major peak shift in the O 1s region of the treated sample indicates that the chemical binding of phosphate oxygen does not change significantly the fluorite structure (i.e., no formation of $CePO_4$[45]). In Figure 4c, the peak at ~529 eV in the emission spectrum is attributed to ceria structural O−Ce bonding and exists in both treated and untreated samples; there is a small shift of this peak at a higher binding energy (~0.3 eV), indicating that the concentration of $Ce^{3+}$ has indeed increased in the treated sample. The intensity of the HO−Ce bonding at ~532 eV is increased and broader in the phosphate-treated sample, which indicates that surface hydroxyl groups play a key role in phosphate ion adsorption. The peak at ~532 eV has also shifted at a higher binding energy (~0.3 eV), indicating again that there is a higher concentration of $Ce^{3+}$ (interacting with hydroxyl groups) after the treatment with phosphate. Indeed weakly bound phosphate interactions can be detected on the surface of nanoceria after treating the material with phosphate buffer solution (Figure 4d), which indicates the nanoparticle surface displays interaction with phosphate due to residual $Ce^{3+}$ oxidation state on its surface. There is now a PO−Ce peak in oxygen binding energies (Figure 4c) after nanoceria has been treated with phosphate; this is seen as a peak at ~531.5 eV. As this peak is not as intense as the O−Ce peak in the treated sample, this is proof that $CePO_4$ has not formed on $Ce^{4+}$-rich nanoceria unlike for $Ce^{3+}$-rich nanoceria.[45]

**Factors Controlling the Phosphate Interaction with Nanoceria.** At the molecular level, we predict that there are three factors that contribute to the phosphate−ceria interaction strength.

The surface hydroxyl concentration has a minor effect on the phosphate−ceria interaction strength. In particular, for oxygen-deficient surfaces with $HO^-$ (Scheme 3), and without $HO^-$ (Scheme 2), there is a minimal change in interaction energy (Figure 2b,c). The hydrogen bonding network seems therefore to have little impact on the adsorption of phosphate on nanoceria.

The surface oxygen vacancy concentration influences considerably the phosphate−ceria interactions. Specifically, the interactions are much stronger when surface oxygen vacancies are present (Schemes 2 and 3) compared to surfaces without oxygen vacancies (Scheme 1). This is regardless of whether the surface is hydroxylated (Scheme 3) or not (Scheme 2).

Surface $Ce^{3+}$ concentration surprisingly does not increase the phosphate−ceria interaction. In particular, the interaction energy remains fairly "flat" as $Ce^{3+}$ increases (Schemes 1 and 3). The only case that we observe a stronger interaction, as the $Ce^{3+}$ concentration increases, is on surfaces that are oxygen-deficient but not hydroxylated (Figure 2b and Scheme 2). Finally, we note that phosphate usually adsorbs on the surface, maximizing its interaction with $Ce^{3+}$.

**Unusual Reconstruction.** Of particular note is phosphate adsorption on the {100} surface (Figure 3b). In particular, the surface oxygen layer on the {111} and {110} surfaces remains highly ordered when phosphate is adsorbed. Conversely, adsorption on the {100} surface results in a large reconstruction, which maximizes the bonding network between surface cerium and phosphate. This reconstruction appears for


DOI: 10.1021/acsabm.8b00709
ACS Appl. Bio Mater. XXXX, XXX, XXX−XXX

all {100} surfaces, whether hydroxylated or oxygen-deficient (hence in all of our schemes studied). The reconstruction is likely due to the flexibility of the {100} surface oxygen network, which can easily access many different surface oxygen arrangements due to very small energy differences between these arrangements, and thus, this surface can easily accommodate adsorbed species, which further stabilizes the surface.[58,59] This is the first time that evidence of this behavior has been found for the adsorption of inorganic anions (i.e., phosphate).

## DISCUSSION

**Implication for Nanotherapeutics.** Like for any application of nanoceria, the biomedical interpretation at the molecular level of the therapeutic action of nanoceria as a potentially important nanozyme requires an understanding of the surface structure and composition, but this time its modification in the context of biologically relevant environments. In this study, we have shown how the presence of phosphate, a common bodily electrolyte, strongly adsorbs and modifies the surfaces of nanoceria, which as noted can mitigate oxidative stress, by buffering some of the most reactive oxygen species (ROS) in cellular environments. This is similar to the poisoning of ceria nanocatalysts exploited or unwanted for other ceria-based technologies, for energy materials of catalysts.[6] Although the mechanisms of reaction of nanoceria with ROS within the cellular environment are somewhat obscure, it is generally accepted that the scavenging of these reactive species follows Scheme 4; superoxide dismutase (SOD) interacts with the superoxide radical $O_2^{\bullet -}$[14,37−39] (Scheme 4a,b) and catalase with hydrogen peroxide $H_2O_2$[13,39−43] (Scheme 4c,d). In analogy, similar mechanisms of scavenging are likely to underpin "clean-air" technologies (i.e., water splitting and three-way catalysis), exploiting the oxygen storage capacity of ceria.[6]

**Scheme 4. Physiological Reactions of ROS in the Presence of Nanoceria**[a]

$$O_2^{\bullet -} + SOD - Ce^{4+} \rightarrow O_2 + SOD - Ce^{3+} \quad (4a)$$

$$O_2^{\bullet -} + 2H^+ + SOD - Ce^{3+} \rightarrow H_2O_2 + SOD - Ce^{4+} \quad (4b)$$

$$H_2O_2 + catalase - Ce^{3+} \rightarrow H_2O + catalase - (O - Ce^{4+}) \quad (4c)$$

$$H_2O_2 + catalase - (O - Ce^{4+}) \rightarrow H_2O + O_2 + catalase - Ce^{3+} \quad (4d)$$

[a](1) Superoxide dismutase. It is a disproportionation reaction where Ce active sites react with two superoxide ions: one is oxidized to molecular oxygen (eq 4a), and the other is reduced to hydrogen peroxide (eq 4b). (2) Catalase. It is a disproportionation reaction where Ce active sites react with two hydrogen peroxide molecules: one is reduced to water (eq 4c), and the other is oxidized to water and molecular oxygen (eq 4d).

From a modeling viewpoint, although still in its infancy, a first-principles simulation can unravel the interaction of radicals with nanoceria.[60−63] However, this approach for exploring the mechanisms controlling enzyme mimetic activities requires detailed knowledge of the species present on the surfaces. Hence, in this work, we targeted the poisoning effect of phosphate on the selective exploitation of nanoceria nanozyme activities.

Experimental work has shown that the highest superoxide scavenging activity is exhibited by $Ce^{3+}$-rich nanoceria,[38] which is active in both neutral and acidic environments,[20] and is retained upon adsorption of some biomolecules and polymers.[37] Conversely, $Ce^{4+}$-rich nanoceria has a stronger catalase activity, which appears to be independent of morphology, i.e., nanorods and nanocubes.[40] Exposure to phosphate[45] poisons SOD activity,[64] but not catalase activity.[41,44] It is thus clear that the presence of phosphate has a selective impact on the enzyme activity.

The simulation results are also supported by XPS, and as the spectra (Figure 4a) show that $Ce^{3+}$ concentration increases upon phosphate adsorption, we can infer that there is indeed a preferential driving force for phosphate to interact with $Ce^{3+}$ active sites at the surface of nanoceria. Indeed $Ce^{3+}$-rich nanoceria has even been shown to undergo structural reconstruction with the $CePO_4$ phase forming.[45] This demonstrates that any enzyme mimetic activity that is catalyzed by $Ce^{3+}$, i.e., SOD, will be inhibited by the presence of phosphate due to steric sequestration of the reactive sites. The strong affinity of phosphate to $Ce^{3+}$ will also block the conversion to $Ce^{4+}$, quenching the redox activity of nanoceria. Experimentation supports this, as unlike $Ce^{3+}$-rich nanoceria, $Ce^{4+}$-rich nanoceria does not show a strong affinity for phosphate; $CePO_4$ does not form on $Ce^{4+}$-rich nanoceria.[41,42,44,45,56,57] The interaction of phosphate with nanoceria also appears to be dependent upon pH (i.e., $HO^-$ concentration) but only for small nanoparticles.[56] Specially, a change in pH results in a change in the surface composition in terms of the concentration of adsorbed hydroxyl species. Our data indicates that there is a variation (sometimes small) in the interaction between phosphate and nanoceria when the concentration of hydroxyl groups increases, but that this is dependent on the surface morphology and oxygen composition (Figure 2a/Scheme 1 and Figure 2c/Scheme 3). Of note is the {100} surface, which shows a less favorable interaction when the concentration of hydroxyl groups increases independently of surface composition (Figure 2a,c). Here, our data is predictive because the experiment has not yet focused on morphological effects. The experiments also support the ab initio data indicating that hydroxyl groups help the phosphate-nanoceria interaction as demonstrated by the change in relative intensity of the Ce−OH and Ce−O peaks after phosphate treatment (Figure 4c). However, the interaction between phosphate and hydroxyl groups appears to be marginal compared to the interaction between $Ce^{3+}$ and phosphate (Figure 2), as the strength of interaction shown by our modeling data is independent of the increase in concentration of $OH^-$ groups (Schemes 1 and 3).

Our modeling data support the experimental evidence (Figure 4c,d) that there is a strong affinity of nanoceria with phosphate, particularly on the {100} surface because of a heavy surface reconstruction (Figure 3b) irrespective of whether the surface is oxygen stoichiometric (Figure 2a, Scheme 1) or oxygen-deficient (Figure 2c, Scheme 3, and Figure 3b). Ceria nanocubes will therefore experience a greater reduction of SOD enzyme mimetic activity in the presence of phosphate, which is independent of surface composition (Scheme 1, 2, or 3). On the other hand, ceria nano-octahedra with a high concentration of hydroxyl groups will offer greater resistance to phosphate adsorption, thus limiting the quenching of SOD activity; the interaction energy is the weakest and only a small


DOI: 10.1021/acsabm.8b00709
ACS Appl. Bio Mater. XXXX, XXX, XXX−XXX

amount of energy would be needed to remove the phosphate (Figure 2a, Scheme 1).

It is worth noting that our data can only shed light on the early stage of phosphate adsorption. In a high phosphate concentration, $Ce^{3+}$-rich nanoceria transforms in cerium phosphate ($CePO_4$), unlike $Ce^{4+}$-rich nanoceria in this study.[41] The precipitation of $CePO_4$ was seen in vitro[41,42,44,45] and in root cells of cucumber plants, where cerium accumulated both as $CeO_2$ and $CePO_4$.[65,66] Future modeling may target the formation of $CePO_4$ by evolving nanoceria surfaces exposed to phosphate.

The interaction of nanoceria with phosphates is also seen in its phosphatase mimetic activity; this is the hydrolysis of the phosphoester bonds. Although we do not aim at proposing a mechanism from ab initio calculations, we consider only the activation of the nanoceria surface due to the interaction with phosphate. The nucleophilic substitution seems to be the more plausible mechanism, underpinning the phosphatase activity, i.e., dephosphorylation of ATP and other organophosphates.[67] Dephosphorylation depends upon the availability of $Ce^{3+}$ [57] although a high oxygen vacancy and low hydroxyl group concentrations on the surface reduce the phosphatase activity;[68] the activation of phosphorus to nucleophilic attack requires surface hydroxyl groups acting as nucleophilic agents.

Our ab initio calculations show that the interaction of phosphate with nanoceria surfaces is stronger when the surfaces are both hydroxylated and oxygen-deficient (Figure 2c, Scheme 3) compared to when they are only hydroxylated (Figure 2a, Scheme 1). Especially, phosphate adsorbs directly on oxygen vacancies (Figure 3c). Such surface anchoring facilitates nucleophilic attack of phosphate with a hydroxyl group (nucleophile).[69] Dephosphorylation was reported to be pH-independent,[70] but morphology-dependent.[67] Our data shows a great variation in the interaction energies within the different surfaces supporting the morphology-dependent adsorption of phosphate with the most favorable interactions exhibited by the {100} oxygen stoichiometric (Figure 2a, Scheme 1) or oxygen-deficient (Figure 2c, Scheme 3) surfaces. The {111} surface is also a good candidate for anchoring the phosphate, but only when the surface is both hydroxylated and oxygen-deficient (Figure 2c, Scheme 3). We can also infer from our experiments that phosphate and $Ce^{3+}$ concentrations cannot be too high at the surface of nanoparticles as nanoceria will otherwise transform into $CePO_4$, thus inhibiting the phosphatase activity. Our modeling also supports the experimentation (Figure 4c) as it shows hydroxyl groups playing an important role in adsorbing phosphates (Figure 2a), although this depends strongly on the presence of oxygen vacancies, which are needed to stabilize the phosphate adsorption at the surface and facilitate the nucleophilic attack (Figure 2c); this is again morphology-dependent.

Although phosphatase mimetic activity of nanoceria is an exciting discovery, there are currently no concrete biological applications. One explanation for this might be that the ceria nanomaterial was not optimized, and therefore, its phosphatase mimetic activity was not detected experimentally. Accordingly, we predict that, to maximize phosphatase mimetic activity, nanoceria should be synthesized with truncated octahedral or cuboidal morphology to maximize the $CeO_2$ {100} surface exposure, together with $Ce^{3+}$, and a high $HO^-$ concentration (Figure 2c, Scheme 3).

## CONCLUSIONS

The exploitation of nanoceria enzyme mimetic activity depends strongly on the nanoscale structure and chemistry of its surfaces. This is as important for any biomedical application of nanoceria as for any other energy technologies.

Density functional theory modeling has provided atomistic insights into the strength of phosphate poisoning, an important bodily ion that can hinder the biological exploitation of nanoceria enzyme mimetic activity. It is indeed likely that the effects shown here also provide insights into the catalytic processes and poisoning (i.e., sulfur poisoning) in "clean-air" or fuel-cell technologies as the ceria nanomaterial will more likely undergo the same mechanisms, i.e., oxygen capture, storage, and release, exploited in each technology.

Oxygen-deficient nanoceria interact strongly with phosphate compared to hydroxylated nanoceria. However, this interaction depends strongly on surface structure, especially, whether nanoceria consist of {111}, {110}, or {100} surfaces.

As the strongest interaction occurs between {100} surfaces and phosphate due to a large surface reconstruction, our data suggest that ceria nanocubes bind phosphate strongly, which will inhibit $Ce^{4+}/Ce^{3+}$ redox and nanozyme activity to a greater extent compared to ceria nano-octahedra comprising {111} surfaces, as these display much weaker interactions with phosphate.

Our simulation provides a prescription for high phosphatase mimetic activity, the nanomaterial should have a polyhedral or cuboidal morphology to maximize exposure of $CeO_2$ {100} surfaces and comprise a high concentration of $Ce^{3+}$ and oxygen vacancies; the pH should be adjusted in preparation of the nanotheraputic, or encapsulated to maintain a local environment (in vivo), to provide a high $HO^-$ concentration.

There is room here for investigating other aspects to this work, notably whether the interaction of phosphate and nanoceria is affected by the presence of ligands and polymers for biocompatible coating, and other biomolecules characteristic of biological media. However, this should constitute the object of further work.

## ASSOCIATED CONTENT

### Supporting Information

The Supporting Information is available free of charge on the ACS Publications website at DOI: 10.1021/acsabm.8b00709.

Details of models and experimental methodology, adsorption of phosphate ions on surfaces of nanoceria, and peak position of XPS spectra (PDF)

## AUTHOR INFORMATION

### Corresponding Author

*E-mail: m.molinari@hud.ac.uk.

### ORCID

Marco Molinari: 0000-0001-7144-6075
Dean C. Sayle: 0000-0001-7227-9010
Sudipta Seal: 0000-0002-0963-3344
Stephen C. Parker: 0000-0003-3804-0975

### Notes

The authors declare no competing financial interest.
All computational data supporting this study is openly available from the University of Huddersfield data archive.



DOI: 10.1021/acsabm.8b00709
ACS Appl. Bio Mater. XXXX, XXX, XXX−XXX

## ■ ACKNOWLEDGMENTS

The following sources are acknowledged for funding: EPSRC (EP/R010366/1); University of Huddersfield; University of Bath; Collaborative Computational Project 5 (CCP5) funded via EPSRC (EP/J010480/1); Balena HPC facility at the University of Bath; Orion Computing facility at the University of Huddersfield; ARCHER UK National Supercomputing Service (http://www.archer.ac.uk) via the HEC Materials Chemistry Consortium funded via EPSRC (EP/L000202, EP/R029431); UK Materials and Molecular Modelling Hub EPSRC (EP/P020194/1).

## ■ REFERENCES

(1) Wei, H.; Wang, E. Nanomaterials with Enzyme-Like Characteristics (Nanozymes): Next-Generation Artificial Enzymes. *Chem. Soc. Rev.* **2013**, *42* (14), 6060−6093.
(2) Balaban, R. S.; Nemoto, S.; Finkel, T. Mitochondria, Oxidants, and Aging. *Cell* **2005**, *120* (4), 483−495.
(3) Dröge, W. Free Radicals in the Physiological Control of Cell Function. *Physiol. Rev.* **2002**, *82* (1), 47−95.
(4) Tong, L. Y.; Chuang, C. C.; Wu, S. Y.; Zuo, L. Reactive Oxygen Species in Redox Cancer Therapy. *Cancer Lett.* **2015**, *367* (1), 18−25.
(5) Andersen, J. K. Oxidative Stress in Neurodegeneration: Cause or Consequence? *Nat. Rev. Neurosci.* **2004**, *10* (7), S18−S25.
(6) Trovarelli, A. *Catalysis by Ceria and Related Materials*. 2nd ed.; Imperial College Press 2013; Vol. *12*, p 1−888.
(7) Karakoti, A.; Singh, S.; Dowding, J. M.; Seal, S.; Self, W. T. Redox-Active Radical Scavenging Nanomaterials. *Chem. Soc. Rev.* **2010**, *39* (11), 4422−4432.
(8) Dong, H.; Du, S. R.; Zheng, X. Y.; Lyu, G. M.; Sun, L. D.; Li, L. D.; Zhang, P. Z.; Zhang, C.; Yan, C. H. Lanthanide Nanoparticles: From Design toward Bioimaging and Therapy. *Chem. Rev.* **2015**, *115* (19), 10725−10815.
(9) Yang, D.; Fa, M.; Gao, L.; Zhao, R.; Luo, Y.; Yao, X. The Effect of DNA on the Oxidase Activity of Nanoceria with Different Morphologies. *Nanotechnology* **2018**, *29* (38), 385101.
(10) Das, S.; Dowding, J. M.; Klump, K. E.; McGinnis, J. F.; Self, W.; Seal, S. Cerium Oxide Nanoparticles: Applications and Prospects in Nanomedicine. *Nanomedicine* **2013**, *8* (9), 1483−1508.
(11) Xu, C.; Qu, X. Cerium Oxide Nanoparticle: A Remarkably Versatile Rare Earth Nanomaterial for Biological Applications. *NPG Asia Mater.* **2014**, *6*, e90.
(12) Walkey, C.; Das, S.; Seal, S.; Erlichman, J.; Heckman, K.; Ghibelli, L.; Traversa, E.; McGinnis, J. F.; Self, W. T. Catalytic Properties and Biomedical Applications of Cerium Oxide Nanoparticles. *Environ. Sci.: Nano* **2015**, *2* (1), 33−53.
(13) Celardo, I.; De Nicola, M.; Mandoli, C.; Pedersen, J. Z.; Traversa, E.; Ghibelli, L. $Ce^{3+}$ Ions Determine Redox-Dependent Anti-Apoptotic Effect of Cerium Oxide Nanoparticles. *ACS Nano* **2011**, *5* (6), 4537−4549.
(14) Heckert, E. G.; Karakoti, A. S.; Seal, S.; Self, W. T. The Role of Cerium Redox State in the SOD Mimetic Activity of Nanoceria. *Biomaterials* **2008**, *29* (18), 2705−2709.
(15) Pulido-Reyes, G.; Rodea-Palomares, I.; Das, S.; Sakthivel, T. S.; Leganes, F.; Rosal, R.; Seal, S.; Fernández-Piñas, F. Untangling the Biological Effects of Cerium Oxide Nanoparticles: The Role of Surface Valence States. *Sci. Rep.* **2015**, *5*, 15613.
(16) Asati, A.; Santra, S.; Kaittanis, C.; Perez, J. M. Surface-Charge-Dependent Cell Localization and Cytotoxicity of Cerium Oxide Nanoparticles. *ACS Nano* **2010**, *4* (9), 5321−5331.
(17) Peng, L.; He, X.; Zhang, P.; Zhang, J.; Li, Y.; Zhang, J.; Ma, Y.; Ding, Y.; Wu, Z.; Chai, Z.; Zhang, Z. Comparative Pulmonary Toxicity of Two Ceria Nanoparticles with the Same Primary Size. *Int. J. Mol. Sci.* **2014**, *15* (4), 6072−6085.
(18) Xia, T.; Kovochich, M.; Liong, M.; Mädler, L.; Gilbert, B.; Shi, H.; Yeh, J. I.; Zink, J. I.; Nel, A. E. Comparison of the Mechanism of Toxicity of Zinc Oxide and Cerium Oxide Nanoparticles Based on Dissolution and Oxidative Stress Properties. *ACS Nano* **2008**, *2* (10), 2121−2134.
(19) Yokel, R. A.; Hussain, S.; Garantziotis, S.; Demokritou, P.; Castranova, V.; Cassee, F. R. The Yin: An Adverse Health Perspective of Nanoceria: Uptake, Distribution, Accumulation, and Mechanisms of Its Toxicity. *Environ. Sci.: Nano* **2014**, *1* (5), 406−428.
(20) Alili, L.; Sack, M.; Karakoti, A. S.; Teuber, S.; Puschmann, K.; Hirst, S. M.; Reilly, C. M.; Zanger, K.; Stahl, W.; Das, S.; Seal, S.; Brenneisen, P. Combined Cytotoxic and Anti-Invasive Properties of Redox-Active Nanoparticles in Tumor-Stroma Interactions. *Biomaterials* **2011**, *32* (11), 2918−2929.
(21) Tarnuzzer, R. W.; Colon, J.; Patil, S.; Seal, S. Vacancy Engineered Ceria Nanostructures for Protection from Radiation-Induced Cellular Damage. *Nano Lett.* **2005**, *5* (12), 2573−2577.
(22) Hirst, S. M.; Karakoti, A. S.; Tyler, R. D.; Sriranganathan, N.; Seal, S.; Reilly, C. M. Anti-Inflammatory Properties of Cerium Oxide Nanoparticles. *Small* **2009**, *5* (24), 2848−2856.
(23) Liu, X.; Wei, W.; Yuan, Q.; Zhang, X.; Li, N.; Du, Y.; Ma, G.; Yan, C.; Ma, D. Apoferritin-$CeO_2$ Nano-Truffle That Has Excellent Artificial Redox Enzyme Activity. *Chem. Commun.* **2012**, *48* (26), 3155−3157.
(24) Rubio, L.; Annangi, B.; Vila, L.; Hernandez, A.; Marcos, R. Antioxidant and Anti-Genotoxic Properties of Cerium Oxide Nanoparticles in a Pulmonary-Like Cell System. *Arch. Toxicol.* **2016**, *90* (2), 269−278.
(25) Cheng, H.; Lin, S.; Muhammad, F.; Lin, Y.-W.; Wei, H. Rationally Modulate the Oxidase-Like Activity of Nanoceria for Self-Regulated Bioassays. *ACS Sensors* **2016**, *1* (11), 1336−1343.
(26) Mandoli, C.; Pagliari, F.; Pagliari, S.; Forte, G.; Di Nardo, P.; Licoccia, S.; Traversa, E. Tissue Engineering: Stem Cell Aligned Growth Induced by $CeO_2$ Nanoparticles in Plga Scaffolds with Improved Bioactivity for Regenerative Medicine. *Adv. Funct. Mater.* **2010**, *20* (10), 1617−1624.
(27) Niu, J.; Azfer, A.; Rogers, L. M.; Wang, X.; Kolattukudy, P. E. Cardioprotective Effects of Cerium Oxide Nanoparticles in a Transgenic Murine Model of Cardiomyopathy. *Cardiovasc. Res.* **2007**, *73* (3), 549−559.
(28) Pagliari, F.; Mandoli, C.; Forte, G.; Magnani, E.; Pagliari, S.; Nardone, G.; Licoccia, S.; Minieri, M.; Di Nardo, P.; Traversa, E. Cerium Oxide Nanoparticles Protect Cardiac Progenitor Cells from Oxidative Stress. *ACS Nano* **2012**, *6* (5), 3767−3775.
(29) Asati, A.; Santra, S.; Kaittanis, C.; Nath, S.; Perez, J. M. Oxidase-Like Activity of Polymer-Coated Cerium Oxide Nanoparticles. *Angew. Chem., Int. Ed.* **2009**, *48* (13), 2308−2312.
(30) Asati, A.; Kaittanis, C.; Santra, S.; Perez, J. M. Ph-Tunable Oxidase-Like Activity of Cerium Oxide Nanoparticles Achieving Sensitive Fluorigenic Detection of Cancer Biomarkers at Neutral Ph. *Anal. Chem.* **2011**, *83* (7), 2547−2553.
(31) Chen, J.; Patil, S.; Seal, S.; McGinnis, J. F. Rare Earth Nanoparticles Prevent Retinal Degeneration Induced by Intracellular Peroxides. *Nat. Nanotechnol.* **2006**, *1* (2), 142−150.
(32) Wong, L. L.; Hirst, S. M.; Pye, Q. N.; Reilly, C. M.; Seal, S.; McGinnis, J. F. Catalytic Nanoceria Are Preferentially Retained in the Rat Retina and Are Not Cytotoxic after Intravitreal Injection. *PLoS One* **2013**, *8* (3), e58431.
(33) Das, M.; Patil, S.; Bhargava, N.; Kang, J.-F.; Riedel, L. M.; Seal, S.; Hickman, J. J. Auto-Catalytic Ceria Nanoparticles Offer Neuroprotection to Adult Rat Spinal Cord Neurons. *Biomaterials* **2007**, *28* (10), 1918−1925.
(34) Heckman, K. L.; DeCoteau, W.; Estevez, A.; Reed, K. J.; Costanzo, W.; Sanford, D.; Leiter, J. C.; Clauss, J.; Knapp, K.; Gomez, C.; Mullen, P.; Rathbun, E.; Prime, K.; Marini, J.; Patchefsky, J.; Patchefsky, A. S.; Hailstone, R. K.; Erlichman, J. S. Custom Cerium Oxide Nanoparticles Protect against a Free Radical Mediated Autoimmune Degenerative Disease in the Brain. *ACS Nano* **2013**, *7* (12), 10582−10596.
(35) Dowding, J. M.; Song, W.; Bossy, K.; Karakoti, A.; Kumar, A.; Kim, A.; Bossy, B.; Seal, S.; Ellisman, M. H.; Perkins, G.; Self, W. T.; Bossy-Wetzel, E. Cerium Oxide Nanoparticles Protect against $\alpha[\beta]$-


DOI: 10.1021/acsabm.8b00709
*ACS Appl. Bio Mater.* XXXX, XXX, XXX−XXX

Induced Mitochondrial Fragmentation and Neuronal Cell Death. *Cell Death Differ.* **2014**, *21* (10), 1622−1632.
(36) Kwon, H. J.; Cha, M. Y.; Kim, D.; Kim, D. K.; Soh, M.; Shin, K.; Hyeon, T.; Mook-Jung, I. Mitochondria-Targeting Ceria Nanoparticles as Antioxidants for Alzheimer's Disease. *ACS Nano* **2016**, *10* (2), 2860−2870.
(37) Karakoti, A. S.; Singh, S.; Kumar, A.; Malinska, M.; Kuchibhatla, S. V. N. T.; Wozniak, K.; Self, W. T.; Seal, S. Pegylated Nanoceria as Radical Scavenger with Tunable Redox Chemistry. *J. Am. Chem. Soc.* **2009**, *131* (40), 14144−14145.
(38) Korsvik, C.; Patil, S.; Seal, S.; Self, W. T. Superoxide Dismutase Mimetic Properties Exhibited by Vacancy Engineered Ceria Nanoparticles. *Chem. Commun.* **2007**, No. 10, 1056−1058.
(39) Celardo, I.; Pedersen, J. Z.; Traversa, E.; Ghibelli, L. Pharmacological Potential of Cerium Oxide Nanoparticles. *Nanoscale* **2011**, *3* (4), 1411−1420.
(40) Pirmohamed, T.; Dowding, J. M.; Singh, S.; Wasserman, B.; Heckert, E.; Karakoti, A. S.; King, J. E. S.; Seal, S.; Self, W. T. Nanoceria Exhibit Redox State-Dependent Catalase Mimetic Activity. *Chem. Commun.* **2010**, *46* (16), 2736−2738.
(41) Singh, S.; Dosani, T.; Karakoti, A. S.; Kumar, A.; Seal, S.; Self, W. T. A Phosphate-Dependent Shift in Redox State of Cerium Oxide Nanoparticles and Its Effects on Catalytic Properties. *Biomaterials* **2011**, *32* (28), 6745−6753.
(42) Singh, R.; Singh, S. Role of Phosphate on Stability and Catalase Mimetic Activity of Cerium Oxide Nanoparticles. *Colloids Surf., B* **2015**, *132*, 78−84.
(43) Kong, L.; Cai, X.; Zhou, X.; Wong, L. L.; Karakoti, A. S.; Seal, S.; McGinnis, J. F. Nanoceria Extend Photoreceptor Cell Lifespan in Tubby Mice by Modulation of Apoptosis/Survival Signaling Pathways. *Neurobiol. Dis.* **2011**, *42* (3), 514−523.
(44) Singh, S. Cerium Oxide Based Nanozymes: Redox Phenomenon at Biointerfaces. *Biointerphases* **2016**, *11* (4), 04B202.
(45) McCormack, R. N.; Mendez, P.; Barkam, S.; Neal, C. J.; Das, S.; Seal, S. Inhibition of Nanoceria's Catalytic Activity Due to $Ce^{3+}$ Site-Specific Interaction with Phosphate Ions. *J. Phys. Chem. C* **2014**, *118* (33), 18992−19006.
(46) Kresse, G.; Hafner, J. Ab-Initio Molecular-Dynamics Simulation of the Liquid-Metal Amorphous-Semiconductor Transition in Germanium. *Phys. Rev. B: Condens. Matter Mater. Phys.* **1994**, *49* (20), 14251−14269.
(47) Kresse, G.; Furthmuller, J. Efficient Iterative Schemes for Ab Initio Total-Energy Calculations Using a Plane-Wave Basis Set. *Phys. Rev. B: Condens. Matter Mater. Phys.* **1996**, *54* (16), 11169−11186.
(48) Perdew, J. P.; Burke, K.; Ernzerhof, M. Generalized Gradient Approximation Made Simple. *Phys. Rev. Lett.* **1997**, *78* (7), 1396−1396.
(49) Dudarev, S. L.; Botton, G. A.; Savrasov, S. Y.; Humphreys, C. J.; Sutton, A. P. Electron-Energy-Loss Spectra and the Structural Stability of Nickel Oxide: An LSDA+U Study. *Phys. Rev. B: Condens. Matter Mater. Phys.* **1998**, *57* (3), 1505−1509.
(50) Molinari, M.; Parker, S. C.; Sayle, D. C.; Islam, M. S. Water Adsorption and Its Effect on the Stability of Low Index Stoichiometric and Reduced Surfaces of Ceria. *J. Phys. Chem. C* **2012**, *116* (12), 7073−7082.
(51) Sayle, T. X. T.; Caddeo, F.; Zhang, X.; Sakthivel, T.; Das, S.; Seal, S.; Ptasinska, S.; Sayle, D. C. Structure−Activity Map of Ceria Nanoparticles, Nanocubes, and Mesoporous Architectures. *Chem. Mater.* **2016**, *28* (20), 7287−7295.
(52) Saraf, S.; Neal, C. J.; Das, S.; Barkam, S.; McCormack, R.; Seal, S. Understanding the Adsorption Interface of Polyelectrolyte Coating on Redox Active Nanoparticles Using Soft Particle Electrokinetics and Its Biological Activity. *ACS Appl. Mater. Interfaces* **2014**, *6* (8), 5472−5482.
(53) Barkam, S.; Ortiz, J.; Saraf, S.; Eliason, N.; Mccormack, R.; Das, S.; Gupta, A.; Neal, C.; Petrovici, A.; Hanson, C.; Sevilla, M. D.; Adhikary, A.; Seal, S. Modulating the Catalytic Activity of Cerium Oxide Nanoparticles with the Anion of the Precursor Salt. *J. Phys. Chem C* **2017**, *121* (36), 20039−20050.
(54) Paier, J.; Penschke, C.; Sauer, J. Oxygen Defects and Surface Chemistry of Ceria: Quantum Chemical Studies Compared to Experiment. *Chem. Rev.* **2013**, *113* (6), 3949−3985.
(55) Huang, X.; Beck, M. J. Determining the Oxidation State of Small, Hydroxylated Metal-Oxide Nanoparticles with Infrared Absorption Spectroscopy. *Chem. Mater.* **2015**, *27* (8), 2965−2972.
(56) Dahle, J. T.; Livi, K.; Arai, Y. Effects of Ph and Phosphate on $CeO_2$ Nanoparticle Dissolution. *Chemosphere* **2015**, *119*, 1365−1371.
(57) Kuchma, M. H.; Komanski, C. B.; Colon, J.; Teblum, A.; Masunov, A. E.; Alvarado, B.; Babu, S.; Seal, S.; Summy, J.; Baker, C. H. Phosphate Ester Hydrolysis of Biologically Relevant Molecules by Cerium Oxide Nanoparticles. *Nanomedicine* **2010**, *6* (6), 738−744.
(58) Sayle, T. X. T.; Molinari, M.; Das, S.; Bhatta, U. M.; Mobus, G.; Parker, S. C.; Seal, S.; Sayle, D. C. Environment-Mediated Structure, Surface Redox Activity and Reactivity of Ceria Nanoparticles. *Nanoscale* **2013**, *5* (13), 6063−73.
(59) Mullins, D. R. The Surface Chemistry of Cerium Oxide. *Surf. Sci. Rep.* **2015**, *70* (1), 42−85.
(60) Xue, Y.; Luan, Q.; Yang, D.; Yao, X.; Zhou, K. Direct Evidence for Hydroxyl Radical Scavenging Activity of Cerium Oxide Nanoparticles. *J. Phys. Chem. C* **2011**, *115* (11), 4433−4438.
(61) Kullgren, J.; Hermansson, K.; Broqvist, P. Supercharged Low-Temperature Oxygen Storage Capacity of Ceria at the Nanoscale. *J. Phys. Chem. Lett.* **2013**, *4* (4), 604−608.
(62) Preda, G.; Migani, A.; Neyman, K. M.; Bromley, S. T.; Illas, F.; Pacchioni, G. Formation of Superoxide Anions on Ceria Nanoparticles by Interaction of Molecular Oxygen with $Ce^{3+}$ Sites. *J. Phys. Chem. C* **2011**, *115* (13), 5817−5822.
(63) Huang, M.; Fabris, S. Role of Surface Peroxo and Superoxo Species in the Low-Temperature Oxygen Buffering of Ceria: Density Functional Theory Calculations. *Phys. Rev. B: Condens. Matter Mater. Phys.* **2007**, *75* (8), 081404.
(64) Kumar, A.; Das, S.; Munusamy, P.; Self, W.; Baer, D. R.; Sayle, D. C.; Seal, S. Behavior of Nanoceria in Biologically-Relevant Environments. *Environ. Sci.: Nano* **2014**, *1* (6), 516−532.
(65) Rui, Y.; Zhang, P.; Zhang, Y.; Ma, Y.; He, X.; Gui, X.; Li, Y.; Zhang, J.; Zheng, L.; Chu, S.; Guo, Z.; Chai, Z.; Zhao, Y.; Zhang, Z. Transformation of Ceria Nanoparticles in Cucumber Plants Is Influenced by Phosphate. *Environ. Pollut.* **2015**, *198*, 8−14.
(66) Zhang, P.; Ma, Y.; Zhang, Z.; He, X.; Zhang, J.; Guo, Z.; Tai, R.; Zhao, Y.; Chai, Z. Biotransformation of Ceria Nanoparticles in Cucumber Plants. *ACS Nano* **2012**, *6* (11), 9943−9950.
(67) Wang, Z.-G.; Bi, W.-Z.; Ma, S.-C.; Lv, N.; Zhang, J.-L.; Sun, D.-H.; Ni, J.-Z. Facet-Dependent Effect of Well-Defined $CeO_2$ Nanocrystals on the Adsorption and Dephosphorylation of Phosphorylated Molecules. *Part. Part. Syst. Char.* **2015**, *32* (6), 652−660.
(68) Dowding, J. M.; Das, S.; Kumar, A.; Dosani, T.; McCormack, R.; Gupta, A.; Sayle, T. X. T.; Sayle, D. C.; von Kalm, L.; Seal, S.; Self, W. T. Cellular Interaction and Toxicity Depend on Physicochemical Properties and Surface Modification of Redox-Active Nanomaterials. *ACS Nano* **2013**, *7* (6), 4855−4868.
(69) Zhao, C.; Xu, Y. Theoretical Investigation of Dephosphorylation of Phosphate Monoesters on $CeO_2$(111). *Catal. Today* **2018**, *312*, 141−148.
(70) Janos, P.; Lovaszova, I.; Pfeifer, J.; Ederer, J.; Dosek, M.; Loucka, T.; Henych, J.; Kolska, Z.; Milde, D.; Opletal, T. Accelerated Dephosphorylation of Adenosine Phosphates and Related Compounds in the Presence of Nanocrystalline Cerium Oxide. *Environ. Sci.: Nano* **2016**, *3* (4), 847−856.


DOI: 10.1021/acsabm.8b00709
*ACS Appl. Bio Mater.* XXXX, XXX, XXX−XXX